doi: 10.1590/S0102-261X1997000300007

ABSORPTION OF SOLAR RADIATION BY WATER VAPOR IN THE ATMOSPHERE. PART II: SENSITIVITY TESTS WITH A GENERAL CIRCULATION MODEL.

E. P. de Souza[1,2], P. L. da S. Dias[2], A. Plana-Fattori[2] & J. C. S. Chagas[3]

The impact of implementing the Chou & Lee scheme for absorption of solar radiation by water vapor in the CPTEC/COLA's General Circulation Model is analyzed in this paper. Comparison with results of the present operational version, which uses the Davies scheme, shows that Chou & Lee scheme leads to more shortwave absorption, thus providing an extra warming of the atmosphere, mainly in the upper troposphere. The changes in the meridional distribution of temperature causes weakening of the subtropical jet in the Southern Hemisphere and strengthening of the Northern Hemisphere jet, which is slightly shifted poleward. The increase of the static stability weakens the meridional circulation cells. The increasing shortwave absorption in the atmosphere decreases the downward shortwave irradiance at the surface. As a consequence, the fluxes of enthalpy and latent heat from the surface are reduced. As a result of all these features, zonal mean precipitation and evaporation are also significantly reduced. Comparison with atmospheric fields reported by the Climate Prediction Center (NCEP/NOAA) shows that the configuration of the large-scale fields is, in a general manner, improved with the use of the Chou & Lee scheme in a monthly integration for January 1997.

Key words: Solar radiation; Water vapor absorption; Atmospheric modeling.

ABSORÇÃO DE RADIAÇÀO SOLAR POR VAPOR D'ÁGUA NA ATMOSFERA. PARTE II: TESTES DE SENSIBILIDADE COM UM MODELO DE CIRCULAÇÃO GERAL - *Neste trabalho é estudado o impacto da implementação, no Modelo de Circulação Geral do CPTEC/COLA, do esquema de absorção de radiação solar por vapor d'água proposto por Chou & Lee. A comparação com resultados da versão operacional atual, que usa o esquema de Davies, mostra que o esquema de Chou & Lee leva a uma maior absorção de radiação de onda curta e conseqüentemente produz um aquecimento adicional, principalmente na alta troposfera. A mudança na distribuição meridional de temperatura causa um enfraquecimento do jato subtropical do Hemisfério Sul e fortalece o jato do Hemisfério Norte, deslocando-o mais para o norte. O aumento da estabilidade estática enfraquece as células de circulação meridional. O aumento da absorção de radiação de onda curta na atmosfera diminui a irradiância descendente à superfície. Como conseqüência, acontece uma redução nos fluxos de entalpia e calor latente da superfície. Como resultado de todos esses aspectos, é observada uma redução significativa na precipitação e na evaporação médias zonais. A comparação com campos atmosféricos analisados pelo Climate Prediction Center (NCEP/NOAA) mostra que a configuração dos campos de grande escala, de modo geral, é bastante melhorada com o uso do esquema de Chou & Lee em uma integração mensal para janeiro de 1997.*

Palavras-Chave: *Radiação solar; Absorção por vapor d'agua; Modelagem numérica.*

[1]on leave from:
Departamento de Ciências Atmosféricas
Centro de Ciência e Tecnologia - Universidade Federal da Paraíba

[2]Departamento de Ciências Atmosféricas
Instituto Astronômico e Geofísico - Universidade de São Paulo
Rua do Matão, 1226 - Cidade Universitária - CEP 05508-900 - São Paulo - SP
Fone: (011)818-4712/4713 - Fax: (011)818-4714
e-mail artemio@model.iag.usp.br

[3]Centro de Previsão de Tempo e Estudos Climáticos
Instituto Nacional de Pesquisas Espaciais
Rodovia Presidente Dutra, Km 40 - CEP 12630-000 - Cachoeira Paulista - SP

INTRODUCTION

Before reaching the Earth's surface, the solar radiation undergoes a series of interactions with gases and particles of the atmosphere. Water vapor is the principal absorber in the spectral region beyond 0.5 μm of the solar spectrum, which represents part of the visible and the infrared solar spectrum (Liou, 1980). Considering the large spatial and temporal variations in concentration of water vapor, one can conclude that, from a modeling viewpoint, absorption of shortwave radiation by water vapor is a fundamental problem. As the absorption of solar radiation by water vapor is largely wavelength-dependent, an explicit calculation of the water vapor optical thickness is currently prohibitive in view of the high computational requirement. The most common solution is to parameterize this absorption, i.e., to reduce the integration to a few terms but keeping the essence of the physics involved in the process.

It is important to point out the relevance of a proper calculation of the heating rates in the general problem of atmospheric modeling. An overestimation (or underestimation) of the local heating sources or sinks can cause lack of accuracy in a numerical forecast. One can argue that the radiative effects are small but, as Gray & Jacobson (1977) pointed out: radiation is a process which is always occurring and its collective effect is not negligible. Moreover, it must be kept in mind that shortwave solar radiation is the primary source of energy for the earth-atmospheric system, and one can expect some climatic impact due to errors in calculated water vapor shortwave absorption.

Plana-Fattori et al. (1998), hereafter referred as Part I, discuss and compare the following schemes for the parameterization of solar heating in the atmosphere: Lacis & Hansen (1974), Davies (1982), Briegleb (1992), Ramaswamy & Freidenreich (1992) and Chou & Lee (1996). A single column model is used in Part I where the heating rates and irradiances for the six first ICRCCM shortwave cases are computed (Ellingson et al., 1991). Comparison with the scheme of Chou & Lee shows that the results obtained with the scheme of Davies present the greatest discrepancy.

A question emerges from the conclusion of Part I: is there any significant impact in a long-term numerical simulation? In the present article, a general circulation model (GCM) is used (the CPTEC/COLA model) and monthly averaged fields are calculated. Results obtained with two contrasting schemes are compared (Chou & Lee versus Davies). A brief description of the model is given in the next section, followed by an analysis of the main results achieved. Concluding remarks and future work are presented in the last section.

DESCRIPTION OF THE MODEL AND SIMULATIONS

For this study is chosen the operational version of the GCM model of the Center for Weather Forecast and Climate Studies (CPTEC/INPE, Cachoeira Paulista, SP) which is a version of the GCM model of the Center for Ocean-Land-Atmosphere Interactions (COLA/IGES, USA) which is described by Kinter et al. (1988) and Sato et al. (1989). The model is run with horizontal spectral resolution T42 and with 18 sigma levels in the vertical. Parameterizations of the subgrid scale physical processes include: surface processes, computed by the Simple Biosphere Model - SiB (Sellers et al., 1986 and Sato et al., 1989); turbulent vertical diffusion performed according to the second-order closure of Mellor & Yamada (1982); shallow non-precipitating cumulus effects calculated following Tiedtke (1984); deep cumulus convection of the Kuo-Anthes type (Kuo, 1974 and Anthes, 1977); large-scale precipitation is calculated by removing supersaturation; longwave radiation transfer calculated according to Harshvardhan & Corsetti (1984), including the efficient-radiation scheme of Harshvardhan et al. (1987) to permit the simulation of the diurnal cycle and the cloud radiation interaction scheme developed by Slingo (1987). The GCM's shortwave radiation scheme is based on that of Lacis & Hansen (1974), adapted by Davies (1982).

In this work, two simulations are performed for a whole month, starting with the analysis valid on January 1st,1997 at 00 UTC. The control simulation is performed by using the CPTEC/COLA's GCM model as described above. The second simulation is performed by replacing the original Davies' scheme by the Chou & Lee (1996) scheme, hereafter referred as the CL experiment, for water vapor absorption of shortwave radiation under cloudless conditions. The reason for this choice is justified from the discussions in part I. The model is allowed to run during the entire month, with time steps of 20 minutes and monthly means corresponding to each case are calculated. The sea surface temperature is the climatological mean for January. Shortwave and longwave irradiances are calculated every hour and 3 hours, respectively.

In discussing the results, it will be closely followed the methodology used by Kinter et al. (1988). In the present work, the mean fields for a period of one month are computed and the differences between the two shortwave radiation schemes are analyzed.

It is stressed here the fact that the analysis is focused on differences between the scheme of Chou & Lee and Davies obtained after an one month integration. The mean results are sufficient to point out the basic differences between the performance of both schemes. Although it can be discussed the advantages and disadvantages of both schemes, the analyses are not sufficient to definitely state which scheme is the best. Nevertheless, there are indications of some improvement with the Chou & Lee scheme.

RESULTS AND DISCUSSION

As discussed in part I, the main difference between the Davies and the Chou & Lee schemes is that the last causes more atmospheric absorption by water vapor and therefore more atmospheric warming should be observed. A latitude-pressure cross section of the zonal mean temperature calculated in the CL experiment (with the scheme of Chou & Lee) is shown in Fig. 1a. All the figures used in this section refer to monthly mean values. Fig. 1b shows the difference between zonal mean temperature of the CL experiment and that of the control run (with the Davies scheme). Warming is effectively obtained with the Chou & Lee scheme (Fig.1b) and this effect is more pronounced in the upper troposphere in both hemispheres, primarily in the summer hemisphere (up to 6 K warmer at approximately 200 hPa between 70 and 80°S). Cooling is observed in the Chou & Lee case only in the lower troposphere near 50°S and 25oN and in the lower troposphere at about 60°N, extending up to 450 hPa. More pronounced cooling (>1K) is found near the North Pole between 700 and 450 hPa. In Part I, it was shown that, at some regions of the troposphere, the scheme of Davies can produce more warming than the scheme of Chou & Lee. However, in a fully nonlinear numerical simulation, one cannot ascribe the cooling effect solely to the radiative forcing: a possible synergism between the radiative forcing and the flow dynamics may induce cooling in some regions. This question will be further explored later.

It is interesting to compare Fig. 1b with Fig. 4.1b of Kinter et al. (1988) which shows the difference between the COLA model summer climatology minus the observed

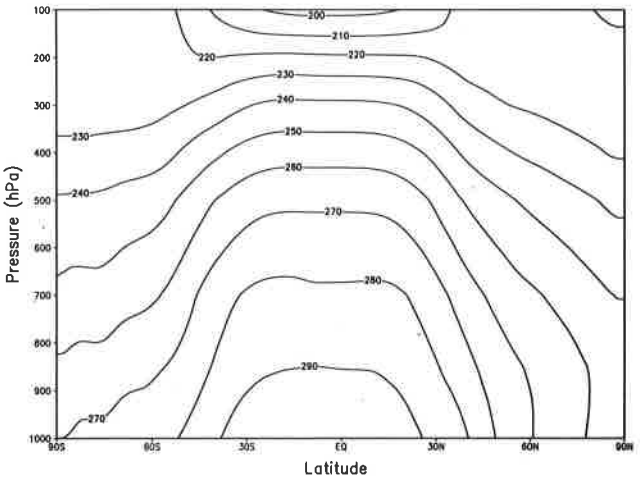

Figure 1a - Zonal mean monthly averaged air temperature in the CL experiment (K).

Figura 1a *- Média zonal da temperatura média mensal do experimento CL (K).*

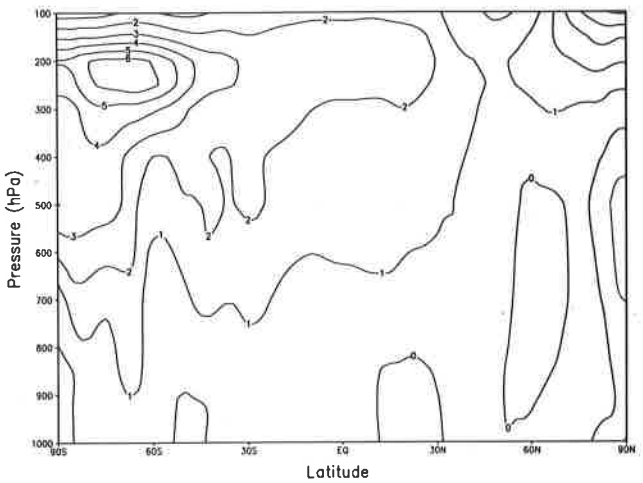

Figure 1b - Zonal mean monthly averaged air temperature, CL minus control run (K). Negative values are dashed.

Figura 1b *- Média zonal da temperatura média mensal, experimento CL menos controle (K). Valores negativos são tracejados.*

analyses. The control model shows a cooling bias primarily in the upper troposphere. Thus, the Chou & Lee scheme helps to decrease the control temperature bias.

Figure 1b shows that the Chou & Lee scheme tends to increase the static stability in comparison with the control run and therefore significant impact may be observed in other mean fields. Figure 2a shows the zonal mean zonal wind of the CL experiment. The typical characteristics of

the mean zonal flow are well described, such as the upper level subtropical jets and easterlies winds in the tropical region. The magnitude of the wind at the jet core is stronger in the Northern Hemisphere, but below the 500 hPa level, the magnitude of the wind is greater in the Southern Hemisphere. Figure 2b shows the zonal mean zonal wind differences between the CL experiment and the control run. The Southern Hemisphere jet is weakened, there is a slight northerly shift of the Northern Hemisphere mid-latitude westerlies and weakening of the polar westerlies. Some improvement has been attained in the Southern Hemisphere simulation considering that the COLA model has a positive bias in the Southern Hemisphere jet intensity (Fig. 4.3b of Kinter et al., 1988). The weakening of the Southern Hemisphere jet can be attributed to the reduction of the meridional temperature gradient due to more warming produced poleward of its core. The slight intensification and the shift of the Northern Hemisphere jet can be attributed to the fact that, in the CL case, more warming occurred in its equatorial side than in its polar one. This differential warming intensified the meridional temperature gradient poleward as compared with the control run. However, in the Northern Hemisphere the changes shown in Fig. 2b do not reduce the COLA model bias (Kinter et al., 1988) except in the polar region.

The zonal mean meridional circulation for the period can be studied through the induced zonal mean vertical

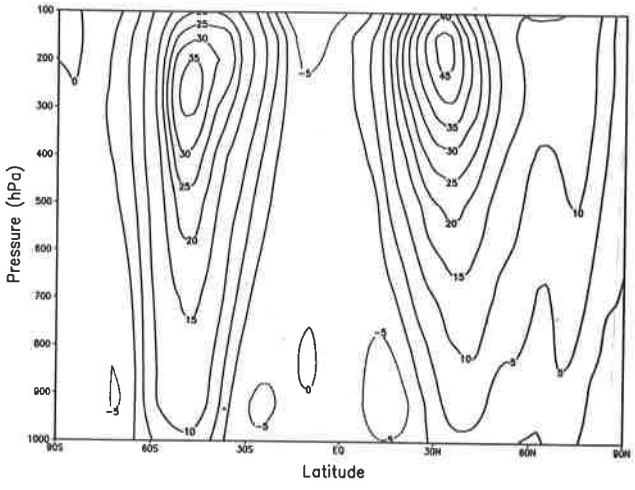

Figure 2a - Zonal mean monthly averaged zonal wind in the CL experiment (m/s).

Figura 2a - *Média zonal do vento zonal médio mensal do experimento CL (m/s).*

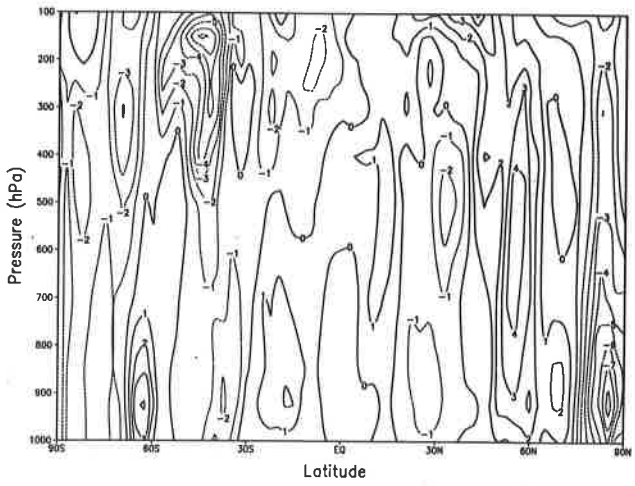

Figure 2b - Zonal mean monthly averaged zonal wind, CL minus control run (m/s). Negative values are dashed.

Figura 2b - *Média zonal do vento zonal médio mensal, experimento CL menos controle (m/s). Valores negativos são tracejados.*

circulation which is shown in Figs. 3a and 3b (Chou & Lee and difference with respect to the control). The main zonal mean upward motion of the Hadley cell is located at approximately 15°S. This region corresponds to the main convectively active areas during this part of the year, such as the convection in the Indian Ocean, the more active areas in the northern part of the South Pacific Convergence Zone (SPCZ) and the South Atlantic Convergence Zone (SACZ). The Ferrel cell is stronger in the Northern Hemisphere as a result of the winter systems imbedded in the highly baroclinic region (Fig. 1a). The weakening of the meridional circulation with the Chou & Lee parameterization is more evident in the Hadley cell, decreasing the maximum upward vertical motion by approximately 20 % (Fig. 3b). Weakening can also be seen in the Ferrel cell in the Southern Hemisphere but a strengthening is observed near the maximum upward movement of the Ferrel Cell in the Northern Hemisphere. The subsidence associated with the descending branch of both Polar cells has intensified in the Chou & Lee case mainly in the North Pole region.

Kinter et al. (1988) conclude that the Hadley and Ferrel cells near the surface in the COLA model resemble the analyzed features but are weaker than analysis near the tropical tropopause. The changes induced by the introduction of the Chou & Lee parameterization reduced the intensity of the Hadley circulation and therefore did not help reducing

the model bias, primarily considering that the Kinter et al. (1988) analysis was not performed with the reanalysis of the NCEP/NOAA (Kousky, 1997) data which tends to show substantial increase in the vertical circulation.

The reduction in the intensity of the Hadley circulation

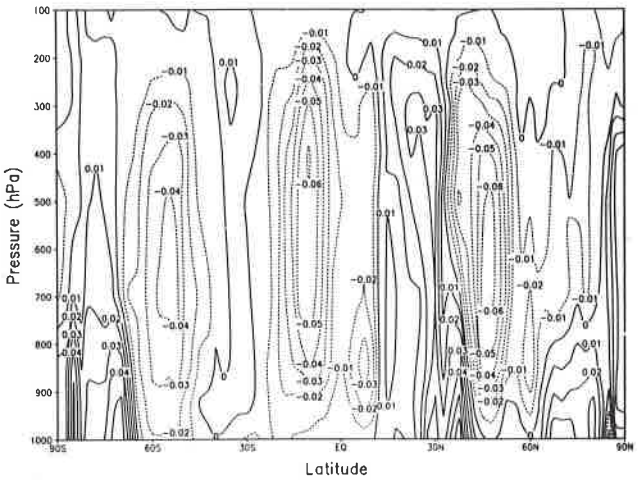

Figure 3a - Zonal mean monthly averaged vertical p-velocity in the CL experiment (Pa/s). Negative values are dashed.

Figura 3a - *Média zonal da velocidade vertical média mensal do experimento CL (Pa/s). Valores negativos são tracejados.*

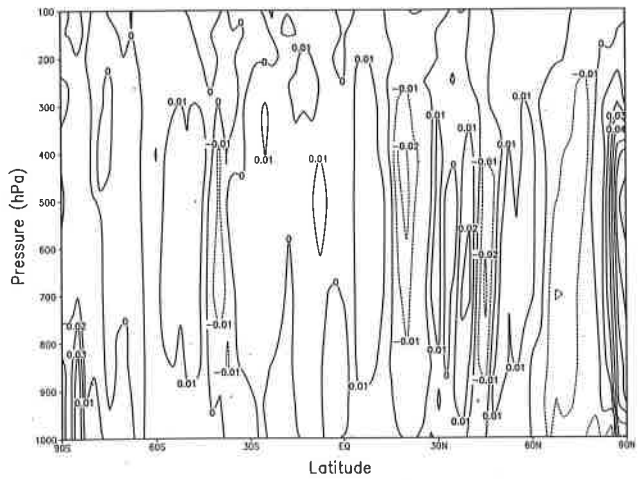

Figure 3b - Zonal mean monthly averaged vertical velocity, CL minus control run (Pa/s). Negative values are dashed.

Figura 3b - *Média zonal da velocidade vertical média mensal, experimento CL menos controle (Pa/s). Valores negativos são tracejados.*

is consistent with the increase of the static stability observed in Fig. 1b (reduction of the intensity of the moist convective forcing). Fig. 4 shows the percent difference between the specific humidity of the CL simulation and that of the control run. It is interesting to observe that Chou & Lee parameterization lead to a slightly moister troposphere, indicating that the observed warming (Fig. 1b) is not completely due the fact that the scheme of Chou & Lee produces more shortwave absorption than the scheme of Davies. Part of this warming must be attributed to the fact that, in the CL case, there is more water vapor to absorb radiation than in the control run.

It is discussed now the impact of the replacement of the scheme of Davies by the scheme of Chou & Lee upon the components of the energy balance of the surface. It is shown in Part I that a reduction in the downward shortwave at the ground should be expected with the use of the Chou & Lee scheme instead of the Davies. Figure 5a (open circles) shows the zonal mean latitudinal distribution of downward shortwave irradiance reaching the ground, for the CL experiment. Fig. 5b (open circles) shows the difference with respect to the control results. The values are zero poleward of 70°N, according to the fact that solar radiation does not reach this region during January. There is an increase in this irradiance southward of 70°N. There is a local maximum of 310 W/m^2 about 35°S and a reduction to a local minimum of 260 W/m^2 at about 60°S. This is in agreement with the expected increase in cloud cover associated with the ascending branch of the Southern Hemisphere Ferrel cell shown in Fig. 3a. Southward of 60°S the shortwave irradiance increases to a maximum of 400 W/m^2 in the South Pole. There is a reduction in shortwave irradiance for all the latitudes southward of 70°N in the Chou & Lee experiment with respect to the control (Fig. 5b). In the Southern Hemisphere, the reduction is greater than 15 W/m^2. This reduction is more pronounced between 30 and 70°S. Recall that this region is moister in the second simulation and more atmospheric absorption must be expected (Fig. 4).

The zonal mean enthalpy flux at the surface and its difference to the control run are shown in Figs. 5a and 5b (squares), respectively. Two local maxima are observed at approximately 30° in both hemispheres. The flux is more intense in the Northern Hemisphere. The sensible heat flux tends to be small or even slightly negative southward of 50°S. Negative flux is also observed northward of 80°N. The Chou & Lee parameterization produces a general

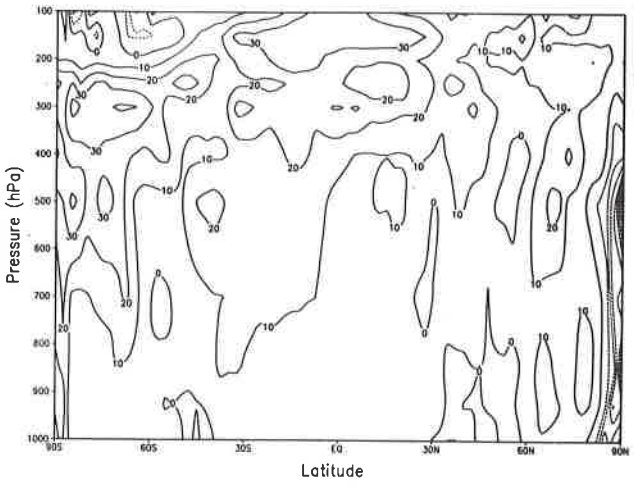

Figure 4 - Percentual difference between the zonal mean monthly averaged specific humidity in the CL experiment and that of the control run (%). Negative values are dashed.

Figura 4 - *Diferença percentual entre a média zonal da umidade específica do experimento CL e a do experimento de controle (%). Valores negativos são tracejados.*

decrease of the enthalpy transfer at the surface southward of 45°N (Fig. 5b). This reduction is coherent with the decrease in the solar radiation forcing at the surface and it is likely to cause less turbulence in the boundary layer. The zonal mean latent heat flux from the surface and its difference to the control run are also shown in Figs. 5a and 5b (closed circles), respectively. There is a reduction in the latent heat flux southward of 45°N in the second simulation. This means that there have been less latent energy available for the saturated convective processes.

It is interesting to observe that northward of 45°N the surface fluxes of heat and moisture have been intensified in spite of the fact that little change was produced in the short wave radiative forcing. The intensification of the baroclinicity in the Northern Hemisphere seems to have increased the westerlies at low levels (primarily between 50 and 70°), thus favoring the intensification of the thermodynamical surface fluxes. The intensification of the baroclinicity in the Northern Hemisphere higher latitudes is clearly shown in the analysis of the zonal mean meridional transport of heat which shows significant increase in northward transport north of 40°N (figures not shown).

The zonal mean of the monthly mean precipitation obtained with the Chou & Lee parameterization and the difference with respect to the control are shown in Fig. 6a and

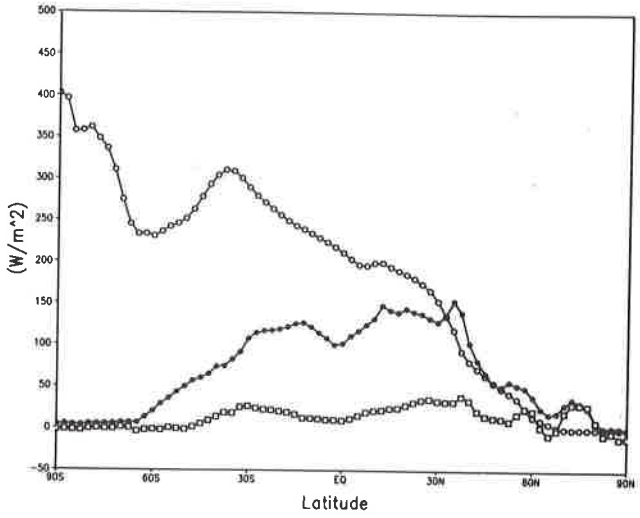

Figure 5a - Zonal mean monthly averaged downward irradiance (open circles), latent heat flux (closed cicles) and enthalpy flux (squares) in the CL experiment (W/m^2).

Figura 5a - *Médias zonais da irradiância descendente (círculos abertos), fluxo de calor latente (círculos fechados) e fluxo de entalpia (quadrados) médios mensais, no experimento CL (W/m^2).*

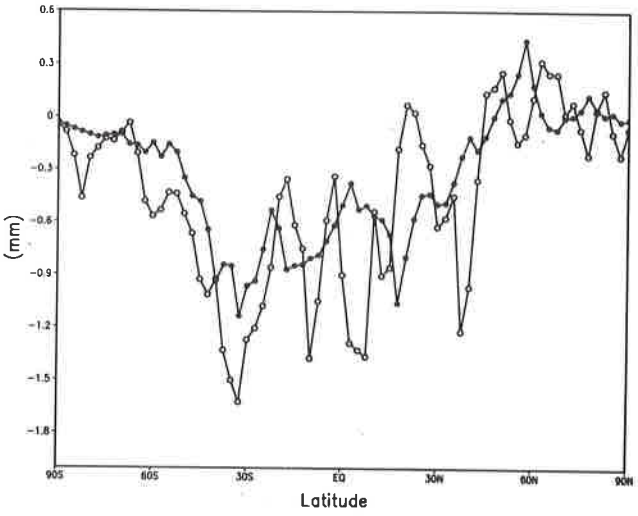

Figure 5b - The same as in Fig. 5a, but for the difference CL minus control run.

Figura 5b - *O mesmo que na Fig. 5a, mas para a diferença CL menos controle.*

6b (open circles), respectively. The main maximum, greater than 7.5 mm/day, is found at approximately 15°S (Fig. 6a). This is consistent with the main ascending branch of the Hadley cell shown in Fig. 3a. Two other local maxima observed in the extratropics are consistent with the ascending branch of

the Ferrel cell in both hemispheres. A clear reduction in precipitation southward of 40 °N and a slight increase northward can be observed in Fig. 6b, in accordance with the discussion in the previous paragraph. Similar behavior can also be observed with the zonal mean evaporation as shown in Figs. 6a and 6b (closed circles), respectively.

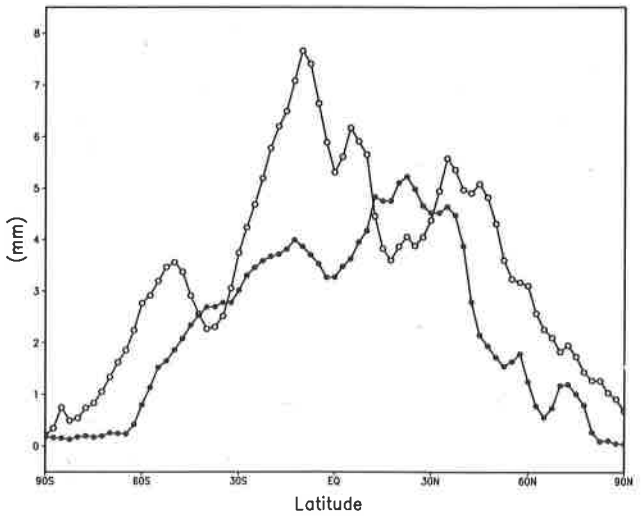

Figure 6a - Zonal mean monthly averaged precipitation (open circles) and evaporation (closed circles) in the CL experiment (mm).

Figura 6a - *Média zonal da precipitação (círculos abertos) e da evaporação (círculos fechados) médias mensais, no experimento CL (mm).*

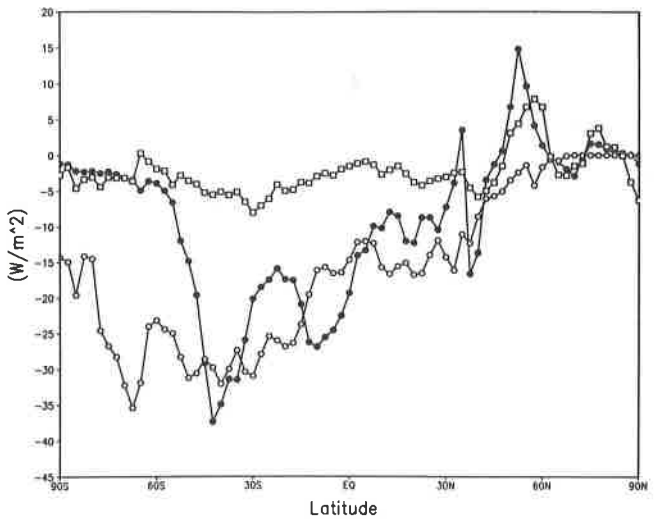

Figure 6b - The same as in Fig. 6a, but for the difference CL minus control run.

Figura 6b - *O mesmo que na Fig. 6a, mas para a diferença: CL menos controle.*

As the scheme of Chou & Lee produces more shortwave absorption and the resultant warming is more pronounced in the upper levels, the atmosphere is likely to be more statically stable. Furthermore, the reduction of the fluxes at the surface tends to reduce the potential of the atmosphere to develop moist convection. One can argue that although in the CL experiment the latent heat flux from the surface is reduced, the atmospheric specific humidity has increased in comparison with the control run, as shown in Fig. 4. This feature can be seen as a consequence that when the convective activity is reduced, the removal of water vapor is also reduced and the atmosphere is able to keep more humidity.

It is worth to consider which impact the scheme of Chou & Lee has in the configuration of the global fields. Toward this goal, it is presented some mean fields calculated with the Chou & Lee scheme, the correspondent fields calculated in the control run and the mean fields reported by the NCEP/NOAA for the same period (January 1997). The monthly mean sea level pressure is shown in Fig. 7. Some features which are not well handled in the control run have been improved in the CL simulation (Fig. 7a). This improvement is more evident in the Northern Hemisphere. The North Atlantic subtropical high, which is underestimated in the control run (Fig. 7b), is better represented in the CL case (Fig. 7a). The intensities of the Subtropical High off the West Coast of North America and of the Aleutian Low in the North Pacific are again best represented in the CL case. The same happens with the Southern Hemisphere subtropical highs. The pressure over the continental regions is represented in a quite similar fashion in both simulations and is in good agreement with the observed mean. A worth-noting feature is the representation, in the Chou & Lee case, of the pressure wave pattern over the Australia (see Fig 7c). This pattern is not well represented in the control run.

The mean 200 hPa velocity potential for the Chou & Lee, control and observed cases are shown in Figs. 8a, 8b and 8c, respectively. There is a reduction in the intensity of the upper level divergence in both model experiments but the CL case shows some improvement. The center of the upper level divergence over tropical South America in the CL experiment (Fig. 8a) is closer to the observed feature (Fig. 8c). The control case tends to show too much upper level divergence over the Andes mountains (Fig. 8b). This seems to be explained by the effective reduction of the upper level static stability in the CL case which tends to inhibits

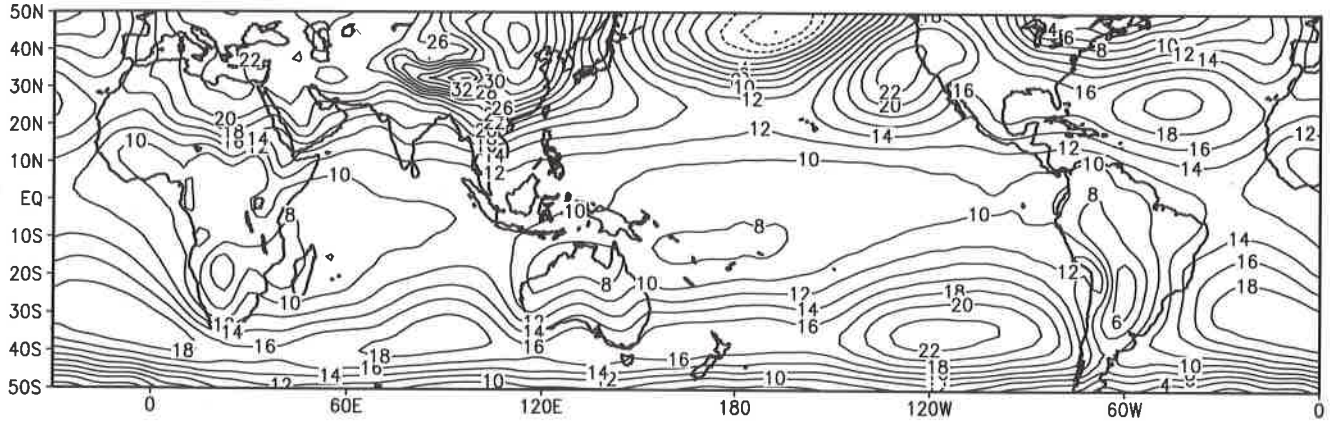

Figure 7a - Monthly mean sea level pressure in the CL experiment (+1000 hPa).

Figura 7a *- Pressão média mensal ao nível do mar no experimento CL (+1000 hPa).*

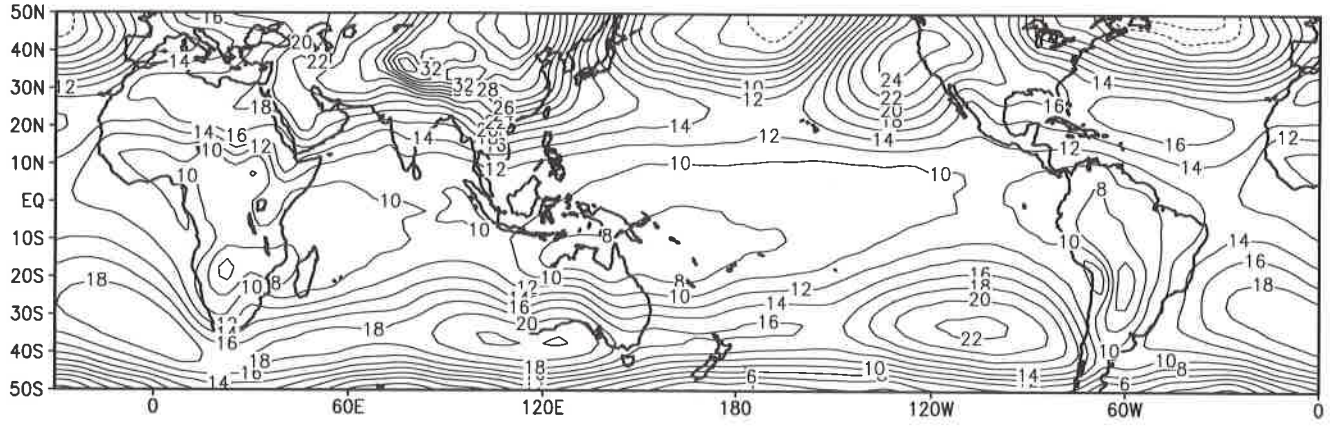

Figure 7b - Monthly mean sea level pressure in the control run (+1000 hPa).

Figura 7b *- Pressão média mensal ao nível do mar no experimento de controle (+1000 hPa).*

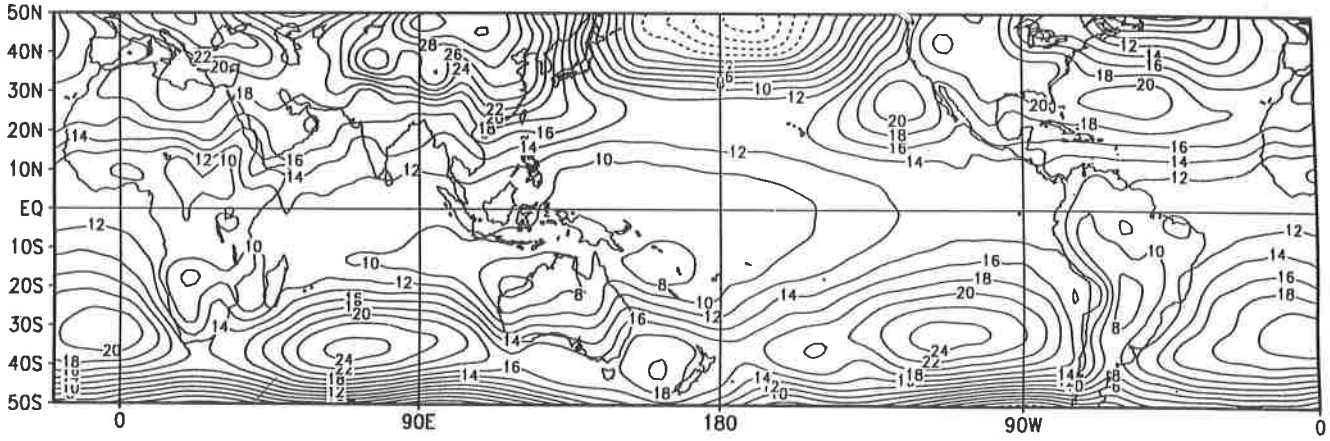

Figure 7c - Observed monthly mean sea level pressure (+1000 hPa), according to Kousky (1997).

Figura 7c *- Pressão média mensal observada ao nível do mar (+1000 hPa), conforme Kousky (1997).*

the extremely deep convection observed in the control case in this area. Another positive change is observed in the eastern Pacific: the control case indicates to much upper level divergence at approximately 15°- 20°N off the west coast of Central America (Fig. 8b compared with Fig. 8c). The CL case (Fig. 8a) indicates much smaller upper level divergence.

The general configuration of the CL upper level velocity potential (Fig. 8a) is closer to the observed field over Africa. However, both model experiments fail to properly reproduce the observed zonal orientation of the upper level divergence in the Indian Ocean. Thus, the model produces excessive upper level divergence over the southern Asian continent. Both model experiments also fail to properly locate the strong observed upper level divergence in the western equatorial Pacific. The Pacific ITCZ and the SPCZ seem weaker than the observed features in both model experiments. In this case, the CL experiment gives weaker upper level divergence than the control although there is a slightly better reproduction of the zonal orientation west of Indonesia (Fig. 8a). The SPCZ in the CL case shows a more zonally oriented upper level divergence east of the date line at approximately 15°S. The observed case indicates a similar feature.

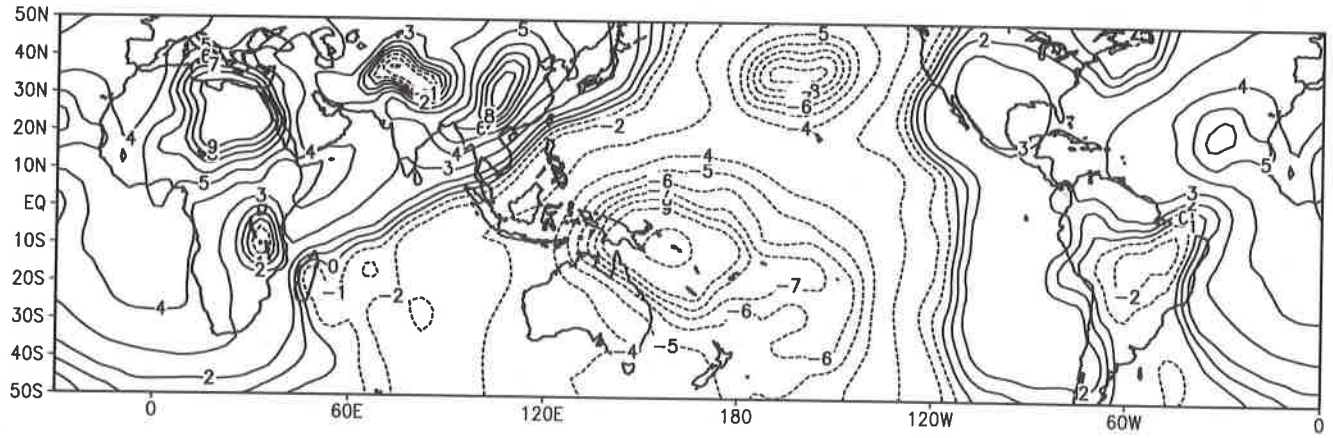

Figure 8a - Monthly mean 200 hPa velocity potential in the CL experiment (10^6 m^2/s).

Figura 8a *- Potencial de velocidade médio mensal em 200 hPa no experimento CL (10^6 m^2/s).*

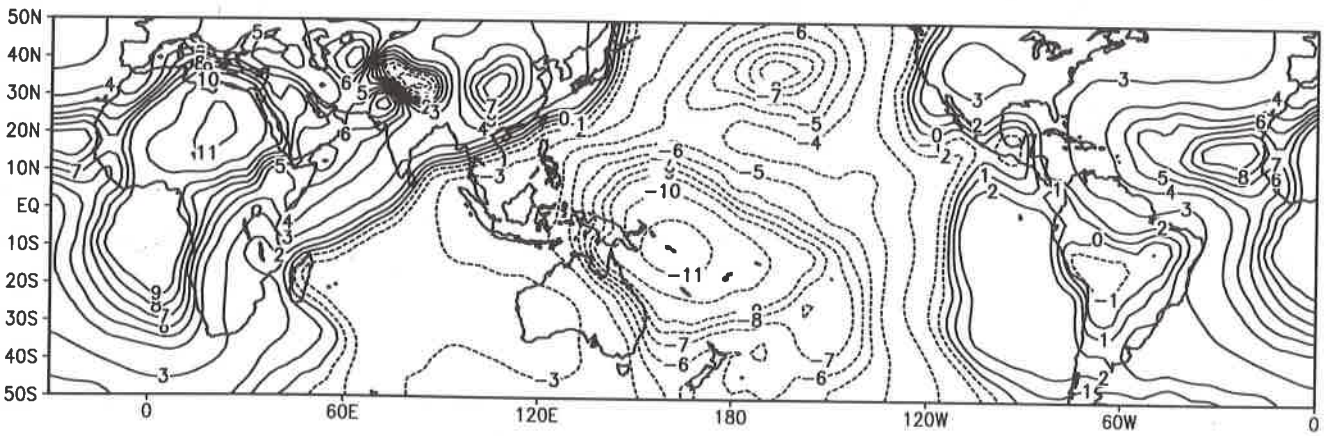

Figure 8b - Monthly mean 200 hPa velocity potential in the control run (10^6 m^2/s).

Figura 8b *- Potencial de velocidade médio mensal em 200 hPa no experimento de controle (10^6 m^2/s).*

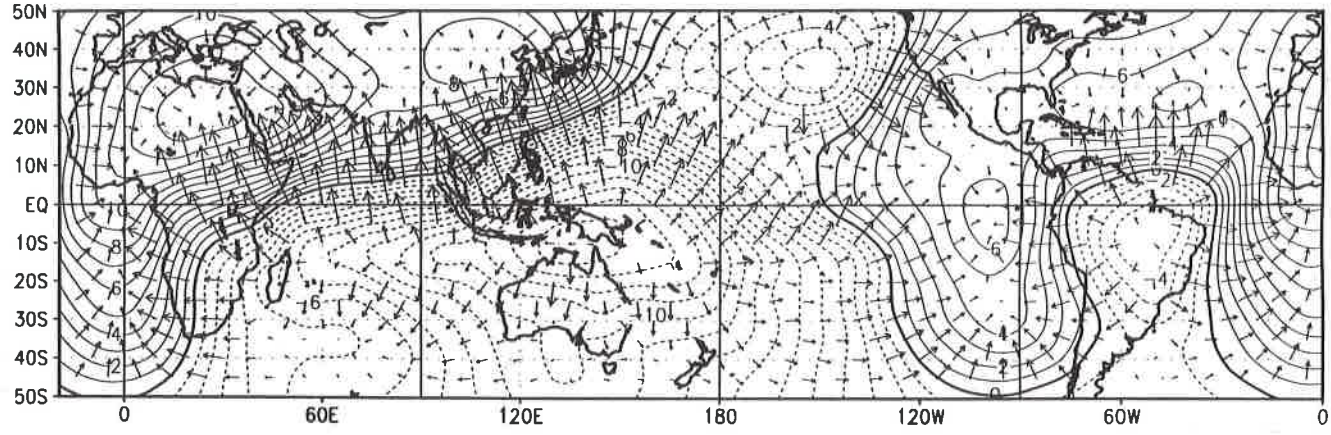

Figure 8c - Observed monthly mean 200 hPa velocity potential (10^6 m^2/s), according to Kousky (1997).

Figura 8c *- Potencial de velocidade médio mensal observado em 200 hPa (10^6 m^2/s), conforme Kousky (1997).*

The upper tropospheric velocity potential is closely correlated with the precipitation primarily in the tropical region. Figure 9 shows the spatial distribution of the Chou & Lee precipitation, control and the Special Sensor Microwave/Imager (SSM/I) precipitation index (NCEP/NOAA; Kousky, 1997). There is a remarkable similarity between the model derived precipitation and the satellite index in most of the area, except in the Indian Ocean where both model experiments overestimate the precipitation north of the equator. The models seem to underestimate precipitation in the tropical continental areas and in the SPCZ/SACZ regions. The eastward shift of the upper level divergence over tropical South America is clearly related to the change in the precipitation pattern. The Chou & Lee precipitation in the SPCZ region is slightly stronger east of the date line, in agreement with the improvement of the upper level circulation described in Fig. 8a. A slight improvement of the precipitation pattern in the northern Indian Ocean is observed with the Chou & Lee scheme, primarily near 60°E. However, both models fail to reproduce the observations in the southern Indian Ocean.

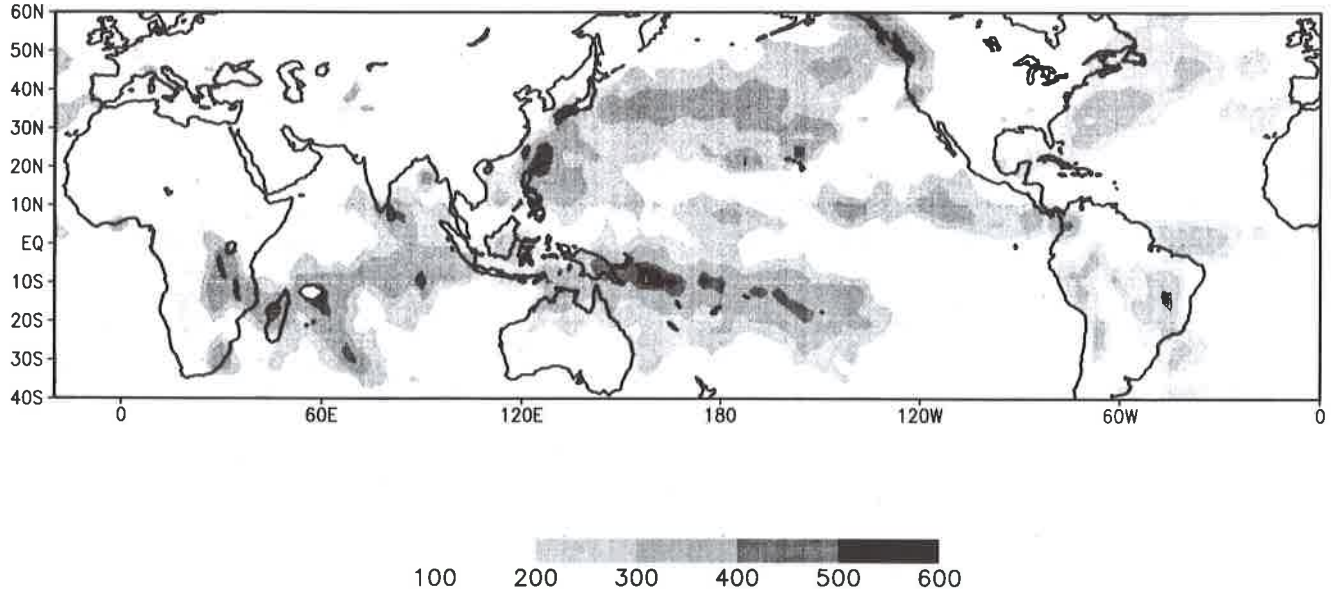

Figure 9a - Accumulated precipitation in the CL experiment (mm).

Figura 9a *- Precipitação mensal acumulada no experimento CL (mm).*

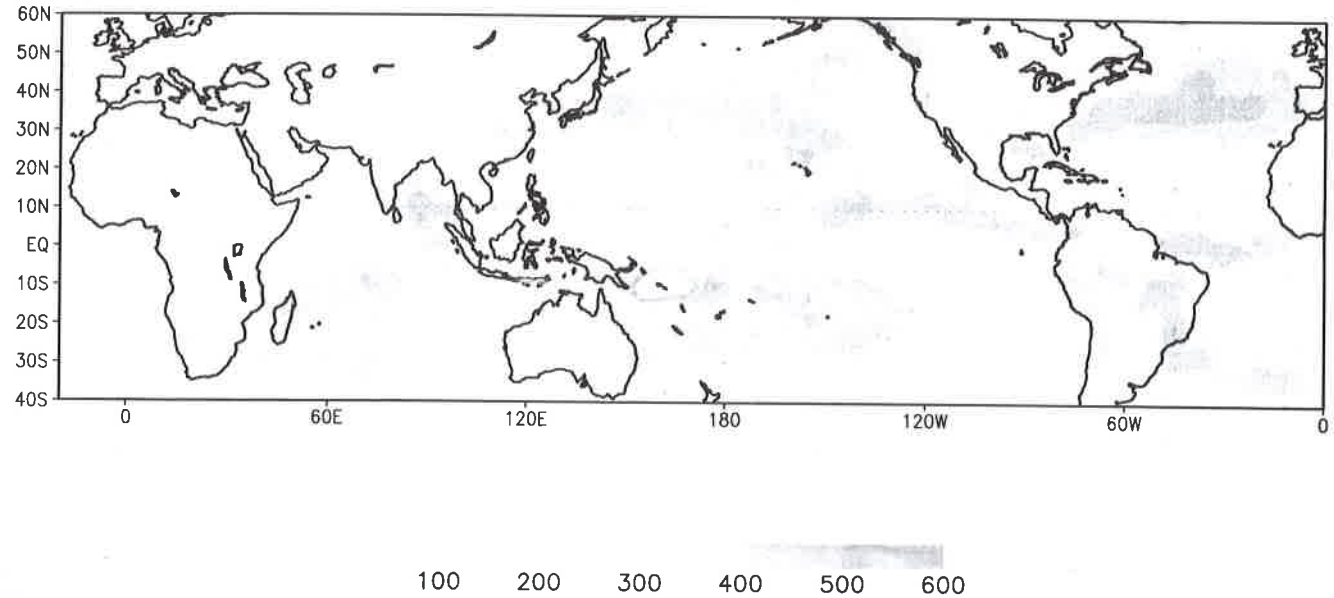

Figure 9b - Accumulated precipitation in the control run (mm).

Figura 9b *- Precipitação mensal acumulada no experimento de controle (mm).*

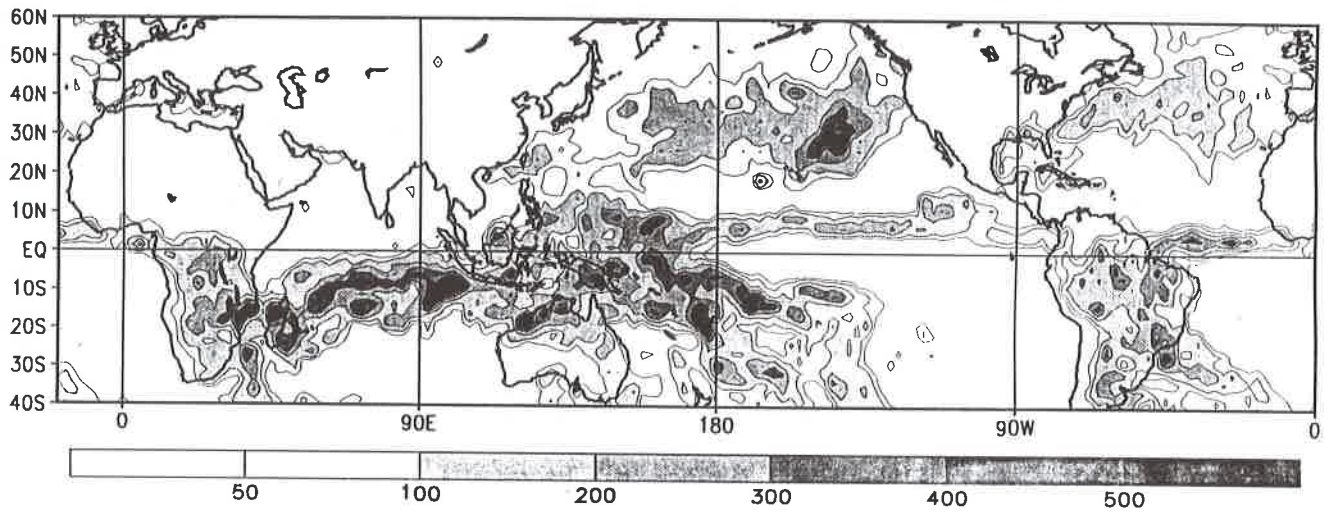

Figure 9c - Observed monthly precipitation (mm), using the SSM/I precipitation index, according to Kousky (1997).

Figura 9c *- Precipitação mensal acumulada observada (mm), usando o índice de precipitação SSM/I, conforme Kousky (1997).*

The monthly mean 200hPa circulation is represented in Fig. 10 in terms of the stream function of the CL experiment (10a), control (10b) and the observed structure (10c). It is interesting to note that the upper level anticyclonic flow north of the equator in the western Pacific seems significantly better reproduced in the CL case (compare Fig. 10a with Fig. 10c). However, the similar feature over the northern Indian Ocean is not reproduced by the CL or control cases. The orientation of the trough in the southern Pacific near 120°W is also better reproduced in the CL case. However, both the strength of the anticyclonic circulation over South America (the Bolivian High) and the similar feature over southern Africa are underestimated. Changes in the upper level divergence certainly have a significant impact in the upper level rotational component of the flow (Grimm & Silva Dias, 1995). The trough off the north-east coast of Brazil in the CL case is better positioned from a climatological point of view. This seems associated with the displacement of the upper level divergence from the Andes in the control case to Central Brazil in the CL case. Gandu & Silva Dias (1998) show that upper level over Central Brazil and along the SACZ is very efficient for generating cyclonic vorticity off the north-east coast of Brazil.

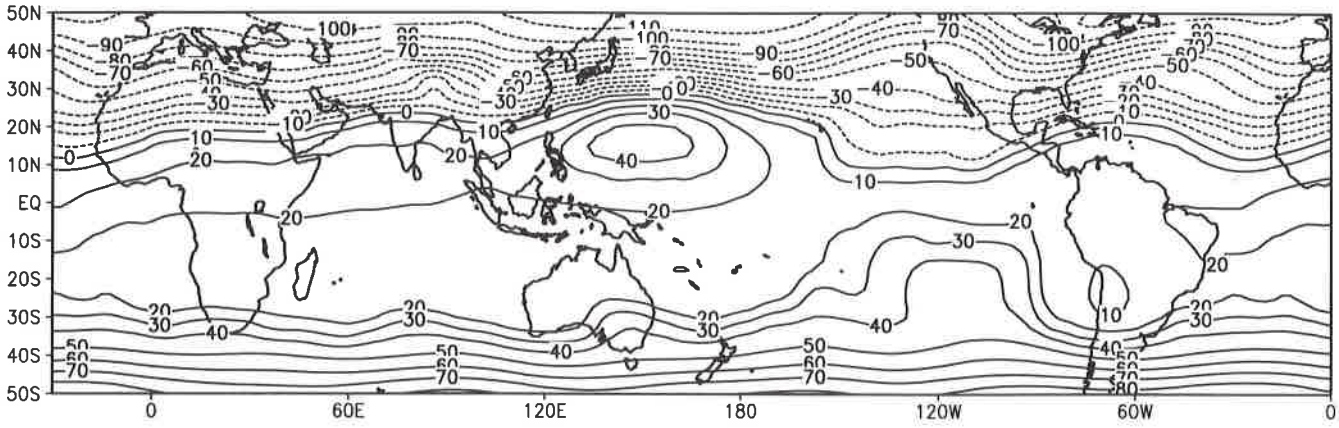

Figure 10a - Monthly mean 200 hPa stream function in the CL experiment (10^6 m^2/s).

Figura 10a - *Função corrente média mensal em 200 hPa no experimento CL (10^6 m^2/s).*

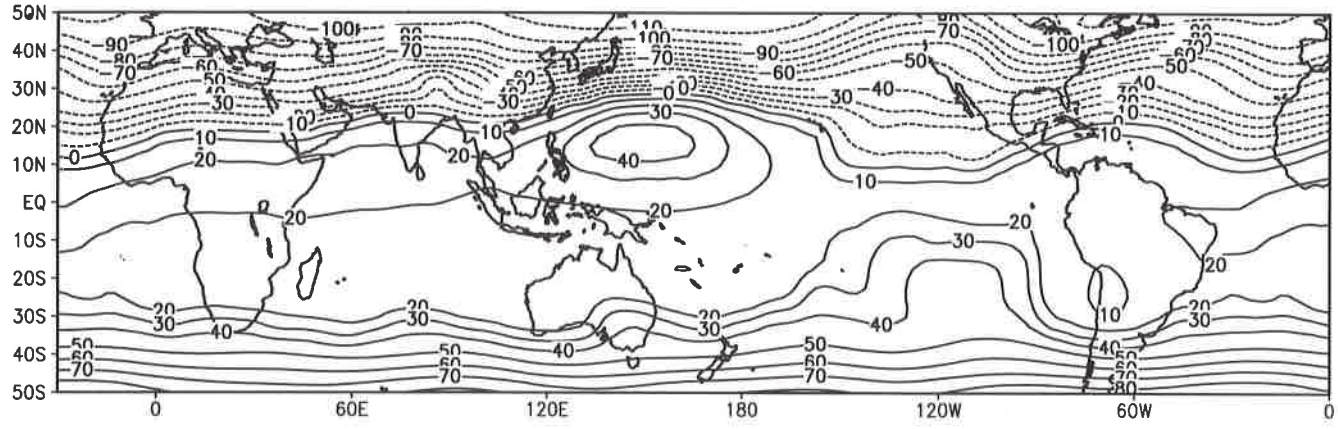

Figure 10b - Monthly mean 200 hPa stream function in the control run (10^6 m^2/s).

Figura 10b - *Função corrente média mensal em 200 hPa no experimento de controle (10^6 m^2/s).*

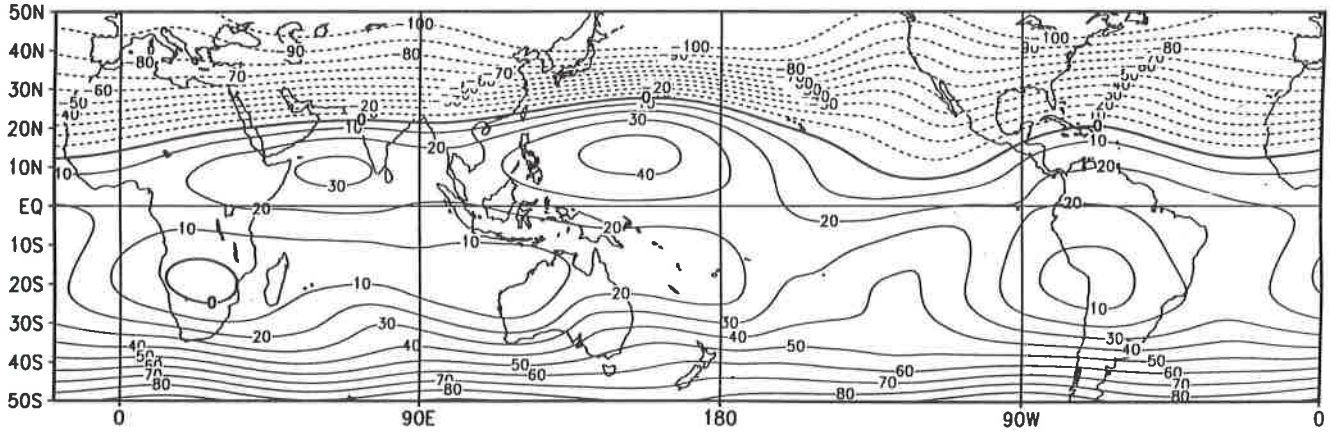

Figure 10c - Observed monthly mean 200 hPa stream function (10^6 m^2/s), according to Kousky (1997).

Figura 10c - *Função corrente média mensal observada em 200 hPa (10^6 m^2/s), conforme Kousky (1997).*

CONCLUDING REMARKS AND FUTURE WORK

In this work, it is compared the numerical simulation of monthly means of several atmospheric variables obtained with two different parameterization schemes of the shortwave solar radiation absorption by water vapor. The control run uses the current operational version of the CPTEC/COLA's GCM with the shortwave absorption by water vapor calculated according to Davies (1982). In the second simulation, this radiative scheme is replaced by the Chou & Lee (1996) scheme, under cloudless conditions.

The use of the Chou & Lee scheme causes more shortwave absorption due to the water vapor absorption and the atmosphere is warmed. This warming is more pronounced in the upper troposphere, mainly in the Southern Hemisphere. An important result obtained by Kinter et al. (1988), using a GCM similar to that of the control run, is that the zonal mean temperature of the upper troposphere is underestimated by some degrees. As the results with the Chou & Lee parameterization lead to warming in the troposphere, primarily at the upper part, and the comparison with some observed fields shows improvement in respect to the control run, there is a clear indication that the temperature bias can be substantially reduced by the use of the Chou & Lee parameterization.

As a consequence of the different meridional distribution of temperature, the Southern Hemisphere subtropical jet is weakened and the Northern Hemisphere subtropical jet is intensified and shifted poleward. The meridional circulation is also generally weakened in the Chou & Lee case. This effect is mainly noted in the Hadley cell and in the Ferrel cell in the Southern Hemisphere. There is a slight increase in the Northern Hemisphere Ferrel cell associated with the increased baroclinicity. The increase in the shortwave absorption in the atmosphere caused decreasing in the downward shortwave irradiance reaching the surface, primarily south of 60°N. As a consequence, the surface sensible and latent heat fluxes are reduced, south of 60°N. The zonal mean precipitation is also reduced by about 15 % in the same area.

The global spatial distribution of the large-scale fields is, in a general manner, better represented in Northern Hemisphere in the CL experiment although some improvement is also observed in the Southern Hemisphere, primarily concerning the location of the highly convective regions over South America and the SPCZ region. Large errors are obtained with both Chou & Lee and control in terms of the spatial distribution of precipitation (and the dynamical variables) in the Indian Ocean and the southern Asian continent. Reasons for these discrepancies are beyond the scope of this paper.

The results obtained in Part I show two distinct groups of schemes, in terms of the heating rates which they produce. One group is obtained with the schemes of Lacis & Hansen (1974) and Davies (1982), as they have the same origin. The other group is formed by the schemes of Briegleb (1992), Ramaswamy & Freidenreich (1992) and Chou & Lee (1996). The additional computing time of implementing the scheme of Chou & Lee is less than 2 %, in comparison with the control run. The reason for choosing the scheme of Chou & Lee was twofold. First, it is the newest among the schemes. Second, the scaling of the water vapor path used in this scheme is somewhat different (see Part I), being conceptually more consistent (Chou & Arking, 1981). These authors argue that the absorption in the line wings, which is more important in the lower troposphere, is more well represented in the way their scaling is performed.

Future work includes a study of the energetics of the circulation and the spin-up problem along the days of integration. Preliminary analyses suggest that there is a reduction of the spin-up and a significant impact in the CL experiment is to be expected on weather forecasting. It is also desirable to test the Chou & Lee parameterization in a climate simulation, running the model up to three or four months.

ACKNOWLEGMENT

The authors would like to thank Mr. Mariano Pereira Silva (CPTEC/INPE) for his help running the CPTEC/COLA's GCM model.

REFERENCES

ANTHES, R.A. - 1977 - Hurricane model experiments with a new cumulus parameterization scheme. Monthly Weather Review, **105**: 270-286.

BRIEGLEB, B.P. - 1992 - Delta-Eddington approximation for solar radiation in the NCAR Community Climate Model. Journal of Geophysical Research, **97(D7)**: 7603-7612.

CHOU, M.-D. & ARKING, A. - 1981 - An efficient method for computing the absorption of solar radiation by water vapor. Journal of the Atmospheric Sciences, **38**: 798-807.

CHOU, M.-D. & LEE, K.-T. - 1996 - Parameterizations for the absorption of solar radiation by water vapor and ozone. Journal of the Atmospheric Sciences, **53(8)**: 1203-1208.

DAVIES, R. - 1982 - Documentation of the solar radiation parameterization in the GLAS climate model. NASA Tech. Memo. 83961, 57p., Goddard Space Flight Center, Greenbelt, MD.

ELLINGSON, R.G., ELLIS, J. & FELS, S. - 1991 - The Intercomparison of Radiation Codes used in Climate Models: long wave results. Journal of Geophysical Research, **96(D5)**: 8929-8953.

GANDU, A.W. & SILVA DIAS, P.L. - 1998 – Impact of tropical heat sources on the south american tropospheric upper circulation and subsidence. Journal of Geophysical Research, **103(D6)**: 6001-6015.

GRAY, W.M. & JACOBSON JR., R.W. - 1977 - Diurnal variation of deep cumulus convection. Monthly Weather Review, **105**: 1171-1188.

GRIMM, A. M. & SILVA DIAS, P. L. – 1995 – Analysis of tropical-extratropical interactions with influence functions of a barotropic model. Journal of Atmospheric Sciences, 52(20): 3538-3555.

HARSHVARDHAN & CORSETTI, T.G. – 1984 – Longwave radiation parameterization for the UCLA/ GLAS GCM. NASA Tech. Memo. 86072, 65p, Goddard Space Flight Center, Greenbelt, MD.

HARSHVARDHAN, DAVIES, R., RANDALL, D.A. & CORSETTI, T.G. - 1987 - A fast radiation parameterization for the general circulation models. Journal of Geophysical Research, **92**: 1009-1016.

KINTER III, J.L., SHUKLA, J., MARX, L. & SCHNEIDER, E.K. - 1988 - A simulation of the winter and summer circulations with the NMC global spectral model. Journal of the Atmospheric Sciences, **45**: 2486-2522.

KOUSKY, V.E. (Ed.) – 1997 – "Climate Diagnostics Bulletin: January 1997". Climate Prediction Center, National Oceanic and Atmospheric Administration.

KUO, H.-L. - 1974 - Further studies of the parameterization of the interactions of cumulus convection on large-scale flow. Journal of the Atmospheric Sciences, **31**: 1232-1240.

LACIS, A.A. & HANSEN, J.E. - 1974 - A parameterization for the absorption of solar radiation in the Earth's atmosphere. Journal of the Atmospheric Sciences, **31**: 118-133.

LIOU, K.-N. - 1980 - An Introduction to Atmospheric Radiation. Academic Press, 392 pp.

MELLOR, G.L. & YAMADA, T. - 1982 - Development of a turbulence closure model for geophysical fluid problems. Review of Geophysics and Space Physics, **20(D4)**: 851-875.

PLANA-FATTORI, A., de SOUZA, E.P. & CHAGAS, J.C.S. - 1998 - Absorption of solar radiation by water vapor in the atmosphere. Part I: A comparison between selected parameterizations and reference results. Revista Brasileira de Geofísica, 15(3): 275-290

RAMASWAMY, V. & FREIDENREICH, S.M. - 1992 - A study of broadband parameterizations of the solar radiative interactions with water vapor and water drops. Journal of Geophysical Research, **97(D11)**: 11487-11512.

SATO, N., SELLERS, P.J., RANDALL, D.A., SCHNEIDER, E.K., SHUKLA, J., KINTER III, J.L., HOU, Y.T. & ALBERTAZZI, E. - 1989 - Effects of implementing the Simple Biosphere Model in a general circulation model. Journal of the Atmospheric Sciences, **46(18)**: 2757-2782.

SELLERS, P.J., MINTZ, Y., SUD, Y.C. & DALCHER, A. - 1986 - A Simple Biosphere Model (SiB) for use within general circulation models. Journal of the Atmospheric Sciences, **43(6)**: 505-531.

SLINGO, J.M. - 1987 - The development and verification of a cloud prediction scheme for the ECMWF model. Quarterly Journal of the Royal Meteorological Society, **113**: 899-927.

TIEDTKE, M. - 1984 - The effect of penetrative cumulus convection on the large-scale flow in a general circulation model. Contributions to Atmospheric Physics, **57(2)**: 216-239.

Submetido em: 25/07/97
Revisado pelo(s) autor(es) em: 20/04/98
Aceito em: 25/04/98

ABSORÇÃO DE RADIAÇÃO SOLAR POR VAPOR D'ÁGUA NA ATMOSFERA. PARTE II: TESTE DE SENSIBILIDADE COM UM MODELO DE CIRCULAÇÃO GERAL

A interação da radiação solar com gases e partículas da atmosfera é um problema fundamental na modelagem de tempo e clima. Plana-Fattori et al. (1998) discutiram o problema da parametrização da absorção de radiação solar por vapor d'água, comparando alguns esquemas e discutindo as suas vantagens. Neste trabalho, é estudado o impacto da implementação, no Modelo de Circulação Geral do CPTEC/COLA, do esquema proposto por Chou & Lee (1996). O modelo é integrado ao longo de janeiro de 1997 e campos médios mensais são obtidos (experimento CL). A comparação é feita com o experimento de controle, no qual a versão operacional atual, que usa o esquema de Davies (1982), é integrada para as mesmas condições.

O principal impacto do esquema de Chou & Lee é observado na distribuição vertical de temperatura. A análise das médias zonais mostram que o aquecimento da alta troposfera tende a ser mais acentuado, corrigindo uma falha do experimento de controle, que tende a resfriar essa região. A nova distribuição meridional de temperatura tende a reduzir a intensidade do jato subtropical do Hemisfério Sul. O jato do Hemisfério Norte fica um pouco mais intenso e deslocado para norte. Como resultado do aumento da estabilidade estática, é observado um enfraquecimento das células de circulação meridional. A célula de Hadley sofre o maior enfraquecimento. Como o esquema de Chou & Lee causa mais absorção na atmosfera, acontece uma redução na irradiância solar que atinge a superfície. Esse efeito é mais intenso no Hemisfério Sul, que é o hemisfério de verão. A diminuição dessa irradiância reduz, substancialmente, os processos energéticos à superfície. O fluxo de entalpia, que define a configuração da camada de mistura e o fluxo de calor latente, que está relacionado à capacidade de desenvolvimento de nuvens convectivas, são reduzidos. Com isso é observada uma redução de aproximadamente 15 % na precipitação média global. Um aspecto interessante é que, como a atividade convectiva, no experimento CL foi reduzida, a atmosfera esteve, em média, mais úmida que no experimento de controle. Isso é um efeito não linear que sugere que parte do aquecimento da atmosfera foi devido ao fato de ela estar mais úmida no experimento CL.

Uma vez que o experimento CL teve o efeito termodinâmico esperado, à luz dos resultados apresentados na Parte I (Plana-Fattori et al., 1998), é interessante que se compare os resultados com algumas observações para que se verifique se houve alguma melhoria no desempenho do modelo. Para isso, são utilizados alguns campos médios, correspondentes ao mesmo período, constantes no "*Climate Diagnostics Bulletin: January 1997*" (Kousky, 1997). A análise da pressão média ao nível do mar mostra que houve uma boa melhoria, principalmente no Hemisfério Norte. A posição e a intensidade dos principais centros de alta pressão assim como a baixa do Pacífico Norte, que não são bem representadas no experimento de controle, aproximam-se bastante do observado no experimento CL. No Hemisfério Sul e sobre os continentes, a melhoria causada pelo esquema de Chou & Lee é mais discreta. Análise do potencial de velocidade em 200 hPa mostra que, no experimento CL, a divergência em altos níveis é, novamente, melhor representada. Isso pode ser verificado sobre a América do Sul Tropical e sobre o Pacífico Leste, ao norte do equador. Mesmo nas regiões onde ambas as simulações falham, como é o caso do Oceano Índico, o experimento CL se aproxima mais da observação. O campo rotacional, dado pela função corrente em 200 hPa, mostra que os cavados e cristas do Hemisfério Norte, assim como o cavado sobre o Nordeste do Brasil, aproximam-se mais do observado no experimento CL. O posicionamento dos principais sistemas convectivos é igualmente bem representado, exceto sobre o Oceano Índico, em ambos experimentos. Entretanto, a redução dos valores máximos de precipitação no experimento CL faz com que os resultados desse experimento se aproximem mais do observado.

Os resultados mostram que a implementação do esquema de Chou & Lee tende a reduzir certos erros produzidos pela pouca absorção atmosférica causada pelo esquema de Davies, principalmente na alta troposfera. Isso faz com que os campos de grande escala calculados com o esquema de Chou & Lee aproximem-se mais dos campos observados.